Risk assessment of ground movements: application to a case study in Lisbon

Mariana Isaura de Moura Ormeche
Instituto Superior Técnico, Universidade de Lisboa
December 2020

Abstract

Geohazards such as landslides, earthquakes, geotechnical risks and floods are a major concern for Lisbon city. This work focus on the analysis of ground movement that could lead to a large scale landslide in the heart of the city before the stabilization works, in an area known as *Miradouro de São Pedro de Alcântara* (MSPA). The MSPA is an emblematic viewpoint in Lisbon embedded in a slope, where increasing displacements were observed in the retaining wall.

To address this subject, the geotechnical parameters of the soil are determined, and the displacements patterns observed of the case study are evaluated to determine whether they represent instability of the slope. Landslide forecasting methods are then used to determine a time of failure for the slope. Finally, the possible causes for these ground movements are established, and a numerical model of the MSPA is developed to confirm the hypothesis for the causes of the ground movement.

Keywords: Landslide, Landslide forecasting methods, Landslide triggering factors, Ground movements

1. Introduction

In general terms, a landslide is described as “a movement of a mass of rock, earth or debris down a slope” (e.g. Cruden, 1991). For Lisbon city, landslides are a major concern in terms of risk. To address this topic, the analysis of ground movement that can may lead to a large scale landslide in the heart of the city before the stabilization works, in an area known as *Miradouro de São Pedro de Alcântara* (MSPA) is the focus of this work.

The analysis of ground movement is first done by determining the geotechnical parameters of the soil, and evaluating the displacements patterns observed of the case study are to determine whether they represent instability of the slope. Landslide forecasting methods are then used to determine a time of failure for the slope. Finally, the possible causes for these ground movements are established, and a numerical model of the MSPA is developed to confirm the hypothesis for the causes of the ground movement.

2. Landslide forecasting methods

Landslide forecasting aims to predict a slope failure in time and/or in space. In this document the focus is in temporal forecast. The most reliable parameters for landslide time forecasting are the slope displacements and its derivatives, velocity and acceleration (Intrieri et al., 2019), as these parameters can be directly related with the stability conditions of the slope (Lacasse & Nadim, 2009).

Over its life time, a slope displacements can be described in a three stages curve (Figure 1): primary stage with displacement increasing logarithmically and strain rate decreasing logarithmically, secondary stage with displacement increasing linearly and constant strain rate and tertiary stage with displacement increasing exponentially and a rapid increase of strain rate.

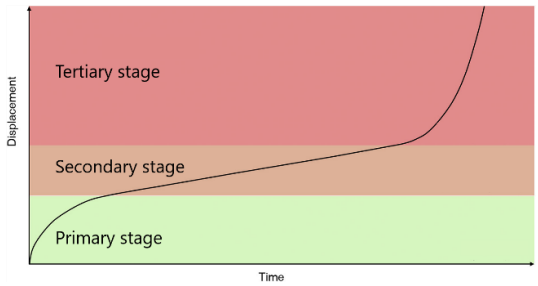

Figure 1. Conventional three state interpretation of creep behaviour (adapted from Intrieri et al., 2019)

Based on kinematic parameters, some empirical methods (e.g. Fukuzono, 1985; Mufundirwa et al., 2010; Saito, 1969) have been developed. These methods have no intrinsic restriction to size, state of activity and type of material (Intrieri & Gigli, 2016), and are usually applied to sliding, toppling and compound landslides. The empirical methods are based on the observation

that displacement velocity increases exponentially before failure. The time of failure is then extrapolated through geometrical arguments from which equations can be derived.

Due to its simpler approach and better results, the Fukuzono (1985) method is the more commonly used and it is the one that is used in this work. The Fukuzono (1985) method consists of plotting the inverse velocity, Λ, versus time, t. If the slope is in equilibrium, the plot will show a line parallel to the time axis, once tertiary stage is reached and the velocity increases asymptotically, the plot will show a decreasing line whose extrapolation intercepts the time axis at the predicted time of failure, t_f.

The inverse velocity, Λ, is then concluded to correspond to equation (1).

$$\Lambda = \frac{1}{v} = [A(\alpha - 1)]^{\frac{1}{(\alpha-1)}}\left(t_f - t\right)^{\frac{1}{(\alpha-1)}} \quad (1)$$

Where A and α are two values found empirically.

For the cases where $\alpha = 2$, the plot is linear and the time of failure, t_f, is determined with linear regression, equation (2).

$$t_f = \frac{t_2\Lambda_2 - t_1\Lambda_1}{\Lambda_1 - \Lambda_2} \quad (2)$$

3. Case study – *Miradouro de São Pedro de Alcântara*

The case study is the MSPA, one of the most emblematic viewpoints of Lisbon, providing a view over the *São Jorge* Castel, Lisbon's downtown and the Tagus River. It is located in the city centre, embedded in *São Roque*'s hill, next to *Bairro Alto* (Figure 2).

Figure 2. Location of the MSPA (adapted from GoogleEarth)

The 1755 earthquake destroyed a large part of Lisbon and the area of the MSPA is then used as a landfill for material resulting from the destruction of the city. In 1770 the construction of two platforms that exist today is conducted. Between 1830 and 1835 landscape works are conducted, turning the area in a public garden (Teixeira Duarte, S.A., 2017).

3.1. Geological conditions

According to the Geological Map of the Lisbon Council, the MSPA is located over *Areolas da Estefânia* (M^1_{II}) and *Argilas e Calcários dos Prazeres* (M^1_{I}) both Miocene formations.

Based on Geotest (2011) site investigation, the *Areolas da Esteania* unit is composed by fine silty sand and silt-sandy clays. The *Argilas e Calcários dos Prazeres* unit is composed by clays, silty clays, fine clayey sands, carbonated marlous clays and limestone, forming a high resistance core.

3.2. Geotechnical conditions

To characterize the geotechnical conditions of the MSPA, data recovered from the geotechnical survey conducted by Geotest (2011) and the surface wave survey conducted by Oliveira (n.d.) are compared in order to define geotechnical zones (GZs) and determine the soil parameters.

The conventional geotechnical survey included five boreholes, S1 to S5, with Standard Penetration Tests (SPTs) and recovery of remoulded samples for visual inspection, and the surface wave survey consisted in the analysis of two acquisition lines of 24 low frequency vertical geophones (4,5 Hz), L1 and L2 with a length of 24 m and 36 m, respectively. The position of the boreholes and the acquisition lines is presented in Figure 3.

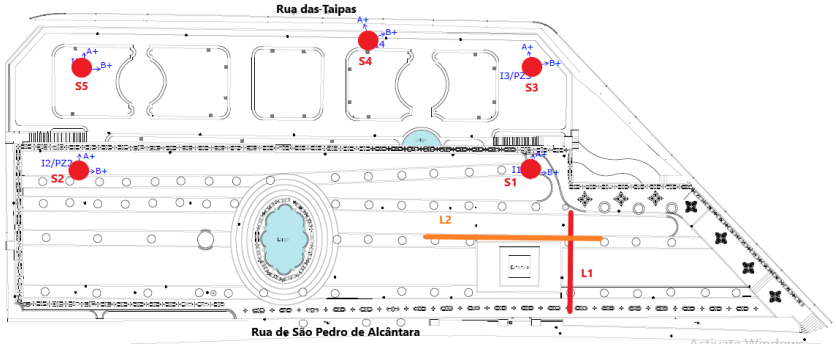

Figure 3. Position of the boreholes, S1 to S5, and the acquisition lines, L1 and L2 (adapted from Geotest, 2011) (unscaled)

Based on the extrapolated SPT test results, three GZs are identified, GZ1 to GZ3. GZ1 has a depth between 10,5 and 16,5 m and a median N_{SPT} of 9, GZ2 has a depth between 25,5 and 34,5 m and a median N_{SPT} of 27, and GZ3 has no identifiable boundary and a median N_{SPT} of 60.

From the surface wave survey, the shear wave velocity, V_S, profile is obtained. From the V_S profile, two GZ are identified: a first GZ with an average depth of 7 m and an average V_S of 350 m/s and a second GZ no identifiable boundary and an average V_S of 550 m/s.

Both with the conventional geotechnical survey and with the surface wave method, two layers were detected. Considering the remoulded samples and the geology of the site, the first layer of both surveys could represent a layer of landfill, and the second layer of both surveys could represent the geological layer *Areolas da Estefânia*. Although no third GZ was identified with the surface wave method, for the geotechnical characterization of the MSPA, GZ3 will also be considered, representing the layer *Argilas e Calcários dos Prazeres*, with no identifiable boundary, and the V_S of GZ3 is determined based on the work of Laranjo (2013) that preformed cross-holes tests between *Cais do Sodré* and *Praça do Comércio* and intercepted the layer *Argilas dos Prazeres*.

Using the correlations proposed by Kulhawy & Mayne (1990), as well as equations (3) and (4), the soil parameters are determined and presented in Table 1.

$$G_0 = \rho V_S^2 \quad (3)$$

$$E_0 = 2(1+\upsilon)G_0 \quad (4)$$

Where G_0 is the initial shear modulus, ρ is the soil's density, E_0 is the initial shear strenght and υ is the Poisson's ratio.

Table 1. Soil parameters

	GZ1	GZ2	GZ3
Field data			
Description	sandy clay with lithic fragments (landfill)	silty and clayey sands, sandy silts (*Areolas da Estefânia*)	limestone and silty clays (*Argilas e Calcários dos Prazeres*)
N^*_{SPT} median	9	27	60
V_S average	350	550	650
γ (kN/m^3)	16	20	25
ρ (ton/m^3)	1,6	2,0	2,5
Data through correlations			
ϕ' (º)	30	35	40
c_u (kN/m^2)	80	200	360
G_0 (kN/m^2)	200 000	586 000	991 000
E_0 (kN/m^2)	480 000	1 410 000	2 377 000

4. Analysis of displacement of the wall

4.1. Topographical monitoring overview

The wall 3D displacements were recorded in two periods: from 2010 until 2012 and from 2017 until 2018, using topographical marks. Sixteen topographical marks (green points in Figure 4) were installed in 2010. N1 to N6 in the East wall and MO1 to MO10 in the North wall.. The three directions in which the displacements were measured were longitudinal (x-direction in Figure 4), transversal (y-direction), and vertical (z-direction).

To ease the identification of trends, a long-term moving average (LMA) is used to smooth the displacement time series, taking 3 values before and 3 after the instant in analysis, thus using $n = 7$ in equation (5):

$$\overline{\delta_t} = \frac{\delta_{t-\frac{n-1}{2}} + \cdots + \delta_t + \cdots + \delta_{t+\frac{n-1}{2}}}{n} \qquad (5)$$

Where, $\overline{\delta_t}$ is the smoothed displacement at time t and δ_t is the registered movement at time t.

Between 2010 and 2012, the longitudinal and vertical displacements of the East and North walls both present sinusoidal variations with a period of one year, presenting no signs of instability, as the trend of the displacements is horizontal. However, the transversal displacements present three patterns of movement (Figure 5). First, in the East wall, the points N1, N3 and N5 present a similar sinusoidal variation as described for the longitudinal displacements. Second, in the East wall, the points N2, N4 and N6 present an increasing displacement, with a maximum cumulative displacement of ~13 mm at the end of 2012. Finally, in the North wall, all the points (MO1 to MO10) move outwards the wall, with a maximum cumulative displacement of ~14 mm at the end of 2012, except for MO8 and MO10 that seem to stabilize at the beginning of 2012.

The displacements measured between 2017 and 2018 are more irregular than the ones between 2010 to 2012, because it includes a single measurement before the construction works and due to those works. Since there is no data from 2012 to 2017, it is not possible to determine if there was a trend change during this time interval or if this irregularity is only due to the construction works. Even though a clear pattern of displacement could not be identified, for either direction, after the end of the construction works, the displacements time history stabilized.

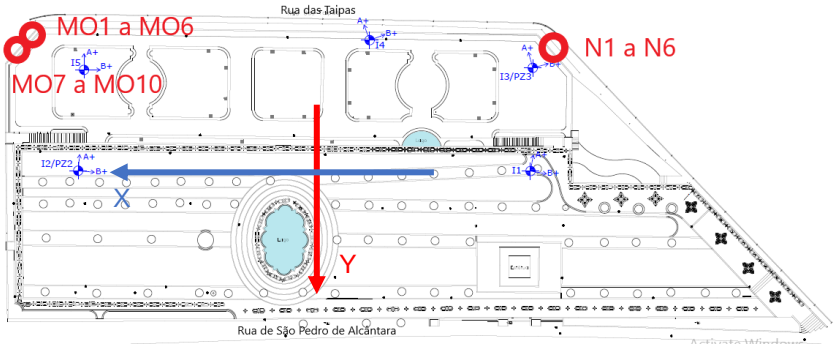

Figure 4. Position of the topographical marks (in green the marks installed in 2010, in red the marks installed in 2017) (adapted from Geoide, 2017) (unscaled)

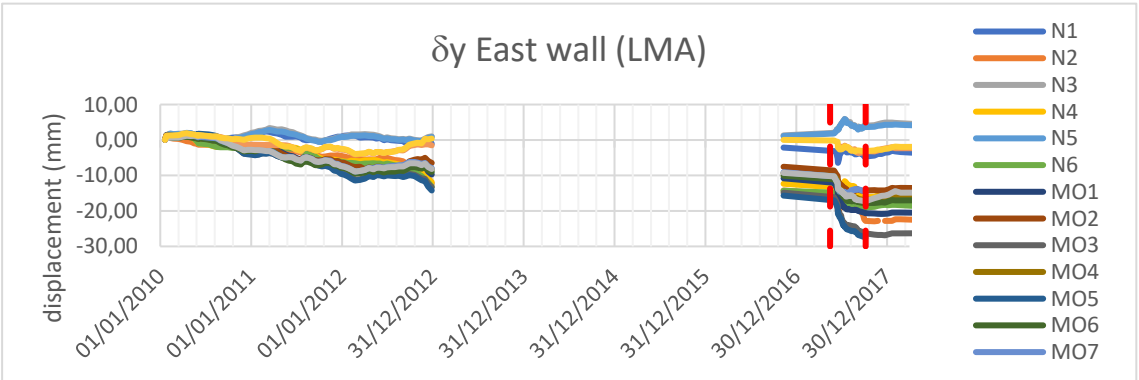

Figure 5. Transversal (δy) smoothed cumulative dispalcements

4.2. Analysis of the inclinometers

Five inclinometers were installed in 2010, I1 to I5 in the SPT boreholes, S1 to S5. This allows the monitoring of lateral displacements with depth. In the displacements measured between 2011 and 2016, the inclinometers from the lower platform (I3, I4 and I5) presented larger displacements in the A axis that corresponds approximately to the transversal direction of the topographical monitoring (§4.1). The displacements measured by these inclinometers are presented in Figure 6 to Figure 8.

In all cases an increment of displacement is observed at a depth of ~24 m that could be related to a slip surface. It should be noticed that for I3 and I4 it corresponds to the interface between the intercepted structures and GZ2, perhaps the structure is sliding. Finally, just like the inclinometers in the upper platform, displacements tend to increase between GZ2 and GZ3, but smother than at 24 m.

Globally, until 2016 the inclinometers show larger displacements at a depth of ~24 m for the inclinometers in the lower platform, right below the intercepted structure in I3 and I4, as well as increased displacements at the interface between GZ2 and GZ3 for all the inclinometers. This can indicate two possible slip surfaces in formation that could explain the increasing displacements of the MSPA.

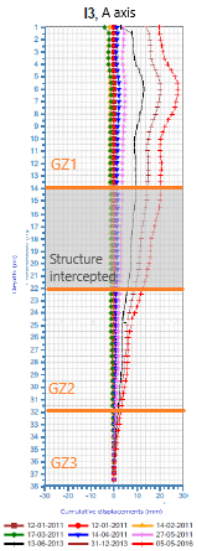

Figure 6. Transversal (δy) cumulative displacement of I3 from 2011 to 2016 (adapted from Geotest, 2016)

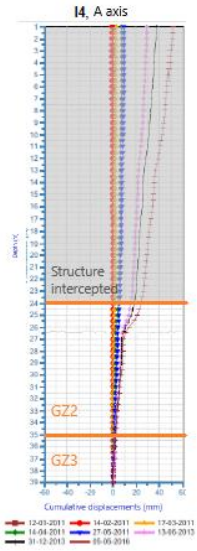

Figure 7. Transversal (δy) cumulative displacement of I4 from 2011 to 2016 (adapted from Geotest, 2016)

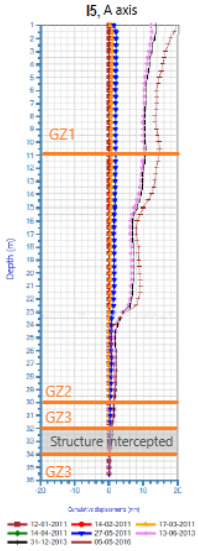

Figure 8. Transversal (δy) cumulative displacement of I5 from 2011 to 2016 (adapted from Geotest, 2016)

4.3. Analysis of possible displacement causes

4.3.1. Precipitation

Precipitation can generate variations in the pore water pressure that may lead to the reduction of effective stresses, reducing the strength of the soil. To understand the effect of precipitation in the MSPA, the precipitation and the displacements are compared between 2010 and 2012. As the effect of rainfall is not instantaneous, the accumulated displacements were compared with the accumulated precipitation for two months (Figure 9).

In all cases the higher values of accumulated precipitation tend to coincide with the larger positive accumulated displacement and the lower accumulated precipitation coincide with the larger negative accumulated displacements. This could indicate a correlation between precipitation and displacements, where displacements increase with precipitation and reduce as the soil dries. It seems as the seasonal component of the displacements captured in the topographical monitoring are due to volume variation induced by precipitation, but do not seem to explain the increasing pattern of displacements.

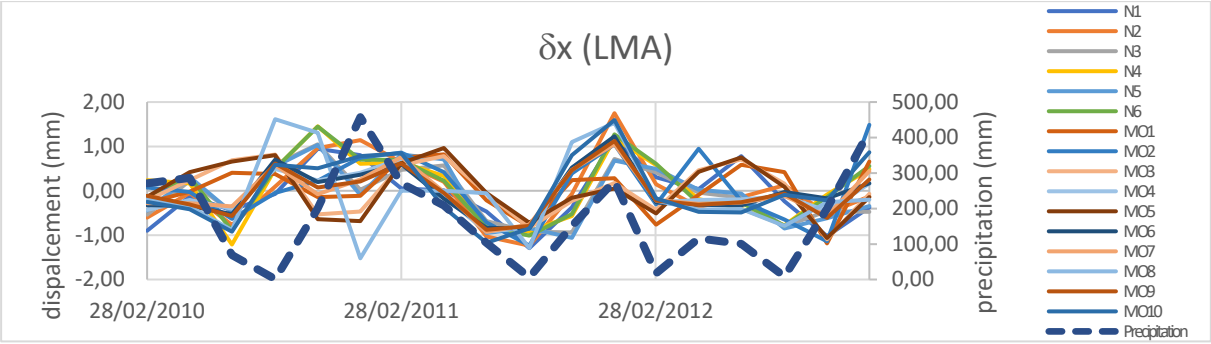

Figure 9. Accumulated longitudinal (δx) displacements and precipitation for two months

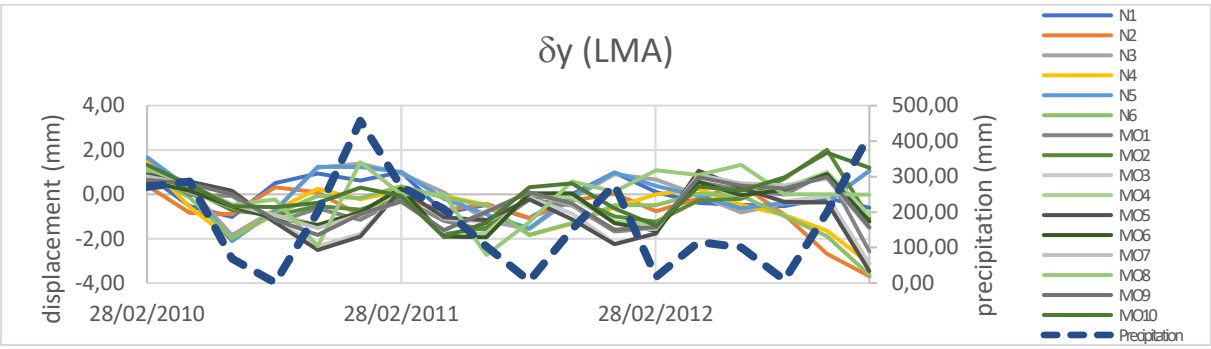

Figure 10. Accumulated transversal (δy) displacements and precipitation for two months

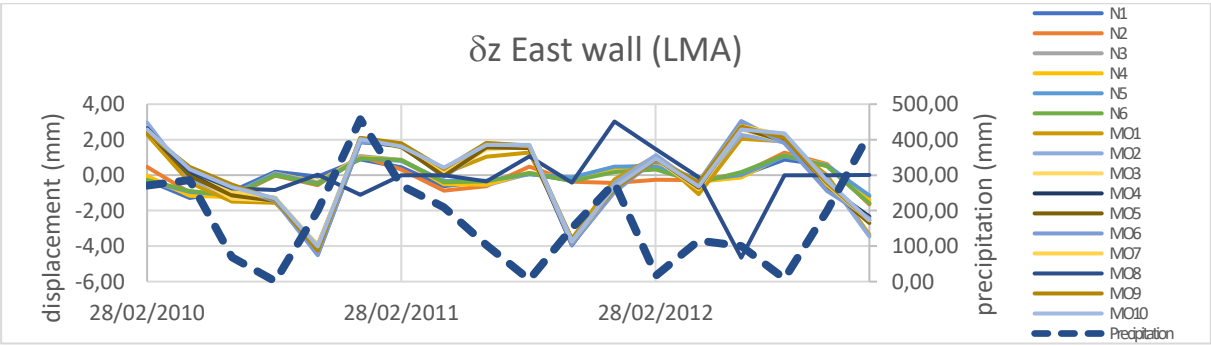

Figure 11. Accumulated vertical (δz) displacements and precipitation for two months

4.3.2. Earthquakes

In the period of analysis of the wall's displacement, a magnitude 4,2 earthquake occurred with a hypocentre at 42 km of the MSPA on the 17/08/2017. However, in all directions, the displacements show a straight line between the measurement made before and after the earthquake, meaning that the earthquake did not seem to have had an impact on the displacements measured.

4.4. Forecasting

The initial aim of this work was to use the displacements measured by satellite to fill the gap between 2012 and 2016 of the topographical monitoring, in order to understand if the trend observed until 2012 changed or not and predict whether the MSPA presented a risk of landslide before the stabilization works, using landslide forecasting methods. As this line of work could not be concluded due to external reasons, the Fukuzono (1985) method is used for the topographical monitoring between 2010 and 2012.

For this analysis only the displacements of the transversal direction are be used, as it is the only direction that presented a pattern of increasing displacement, and the point with the larger cumulative displacement is selected: MO5 in the North wall (~11 mm). As this analysis aims to predict a time of failure, a different LMA was used to smooth the displacement time series, taking 6 values before the instant in analysis, $n = 7$ in equation (6).

$$\overline{\delta_t} = \frac{\delta_{t-n} + \cdots + \delta_t}{n} \qquad (6)$$

As the parameters A and α of the Fukuzono (1985) method (equation 1) are not known, $\alpha = 2$ is considered to perform a linear regression to determine a possible time of failure.

The inverse velocity from December 2011 to December 2012 is plotted in Figure 12. The points where a decreasing trend of the inverse velocity at the end of the measurements is observed are highlighted in red, this decreasing trend are observed between three months before the end of the time series.

Generally, the Fukuzono (1985) method can be an advantage to prevent life and material losses in case of a real landslide in the MSPA area. However, as it has been seen with the analysed points above, it is necessary to be cautious using the values of inverse velocity. In fact, with the predicted time of failure observed in Figure 12 is a false alarm, as the MSPA has not failed until 2017 when stabilization works were performed.

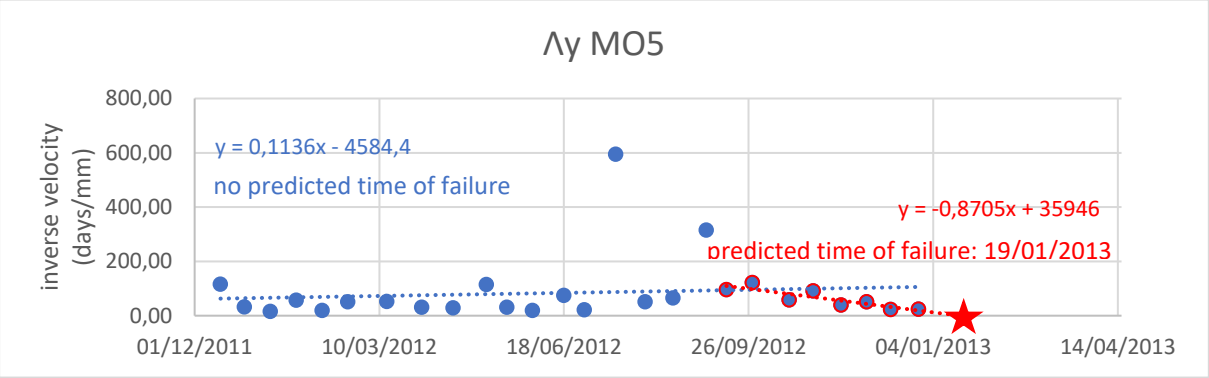

Figure 12. Inverse velocity of MO5 form December 2011 to December 2012[1]

5. Numerical modelling

5.1. Model parameters

To simulate the response of the MSPA, the PLAXIS 2D program based on the finite elements method is used. In this section, the constitutive model used, and the model parameters are introduced, as well as the model geometry. Afterwards, a sensitivity study where several causes are individually studies to try to identify the cause that better match the displacements measured in the MSPA, namely: softening of the interface between geotechnical zones and earthquake loading.

The finite element model simulates the MSPA in the transversal direction, in a cross-section that has exhibited larger displacements and intercepts two inclinometers.

Because the displacement level measured in the MSPA is small, in this work was adopted the Hardening Soil with small strain-stiffness model (HSsmall), since it simulated more accurately the stiffness of the soil in the small strain range. The parameters used in the model are presented in Table 2.

Table 2. Model parameters

	GZ1	GZ2	GZ3
Soil parameters			
γ_{unsat} (kN/m³)	16	20	25
γ_{sat} (kN/m³)	16	20	25
ϕ' (º)[1]	30	35	40
c' (kN/m²)[1]	0	0	0
c_u (kN/m²)[2]	80	200	360
Parameters for soil stiffness			
E_{50}^{ref} (kN/m²)	227 000	307 000	486 000
E_{oed}^{ref} (kN/m²)	227 000	307 000	486 000
E_{ur}^{ref} (kN/m²)	680 000	921 000	1 458 000
Parameters to describe soil behaviour in the small strains range			
G_0^{ref} (kN/m²)	3 780 000	511 000	809 000
$\gamma_{0.7}$ (-)	$4{,}0 \times 10^{-5}$	$8{,}3 \times 10^{-5}$	$8{,}1 \times 10^{-5}$

[1] parameters used for drained analysis
[2] parameters used for undrained analysis

[1] 01/12/2011 corresponds to 40878

For the masonry retaining walls, nonspecific test was performed. To model the retaining walls of the MSPA a linear elastic is used with typical parameters for the material, presented in Table 3.

Table 3. Parameters of the retaining walls

γ (kN/m^3)	22
E (kN/m^2)	30×10^6
ν (-)	0,3

5.2. Simulation sequence

The hypotheses presumed to explain the displacements measured in the MSPA are, as discussed in §4.2, two possible slip surfaces: one between GZ2 and GZ3 and another one between GZ2 and the lower retaining wall, named interface 1 and interface 2, respectively. These hypotheses are simulated by modelling the following cases:

A. Movement along interface 1
B. Movement along interface 2
C. Movement along both interfaces

To model the softening interface effect, the strength reduction factor, R_{inter}, reduced from 1 to 0,7 and 0,5 assess its impact on the displacements in the MSPA.

Due to the uncertainty on the type of load, saturation level, and grain size distribution of the soils in the MSPA area, the simulations are done assuming drained and undrained responses, to determine which behaviour better fits the response of the MSPA.

Additionally, a pseudo-static analysis is preformed to evaluate the stability of the MSPA under seismic action.

5.3. Simulation results

5.3.1. Comparison of the cases A, B and C

From cases A, B and C, the one that presented a displacement trend more similar to the one observed in the MSPA is the case A where the undrained behaviour and $R_{inter} = 0{,}7$ are considered.

This results in displacement mechanism described by a compound slip surface: planar bellow the MSPA and circular after the lower retaining wall, with larger displacements concentrated in the lower platform and GZ1 (Figure 13)

However, the model does not explain the amplitude of the displacements, meaning that the displacements are originated not only by the softening of the interface but also by actions other than a frequent service load over the MSPA area (1 kN/m^2). Additionally, the strength reduction at the interface GZ2/GZ3 seems to generate sharp displacements at that area rather than a linear increase of displacement in that area what could explain this increase of displacement throughout GZ2 could be a stiffness reduction of the layer.

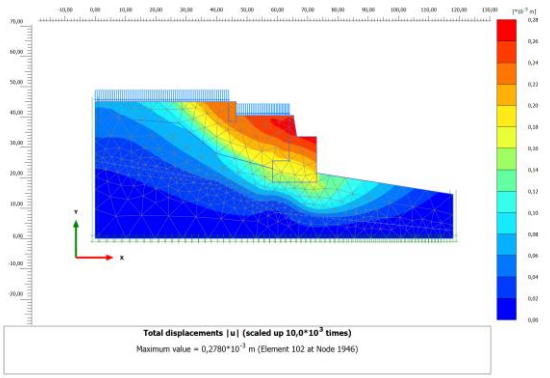

Figure 13. Case A - calculated total displacements for undrained behaviour and $R_{inter} = 0{,}7$

5.3.2. Analysis of stiffness reduction in GZ2

The stiffness parameters of GZ2 were determined using the average V_S. But, based on the analysis of the inclinometers profile, it was decided to test the hypothesis of GZ2 with lower stiffness. Several Vs values were tested, and it was identified that when $V_S = 300\ m/s$ and considering undrained behaviour, the results were the ones that better fit the displacements measured in the inclinometers (Figure 14).

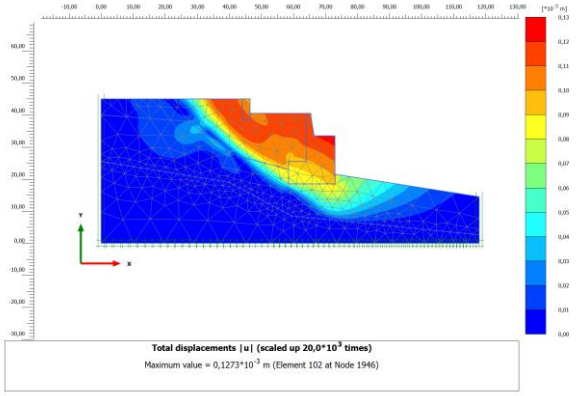

Figure 14. Calculated total displacements for $V_S = 300\ m/s$ in GZ2 with undrained behaviour

As for cases A, B and C the calculated displacements did not reach the amplitude of the measured displacements Yet, the trend of the calculated displacements is similar to the trend of displacements observed, as a linear increase of displacement at the interface GZ2/GZ3 is present now. Additionally, a similar compound slip surface is obtained.

5.3.3. Seismic action (pseudo static analysis)

To analyse the effect in the MSPA of the M4,2 earthquake occurred on the 17/08/2017, a pseudo static-analysis was conducted in the undrained model of the MSPA, as it is the one that better represents the behaviour of the MSPA. For that a horizontal acceleration of 0,004g, that was the maximum acceleration measured in the nearest seismic station (IPMA, n.d.), was applied to the model considering the effect of no interface and of interface 1.

The total displacements a present similar pattern as the displacements presented in §5.3.1, and both show larger displacements in the lower platform and in GZ1, as well as a similar compound slip surface, planar bellow the MSPA and circular after the lower retaining wall. Nevertheless, the acceleration of 0,004g does not lead to major displacements in MSPA. For both cases the maximum displacement is equal to ~0,2 mm, indicating that the interface 1 has no particular effect on the displacements in case of horizontal displacement.

The horizontal acceleration is then increased until the model reaches failure. Failure was only obtained for a horizontal acceleration of 0,50g, that corresponds to an earthquake of a magnitude higher than 9. As interface 1 does not seem to have an impact in the MSPA stability in the case of an earthquake, the analysis was only preformed for the case where no interfaces are considered. The total displacement distribution is presented in Figure 15.

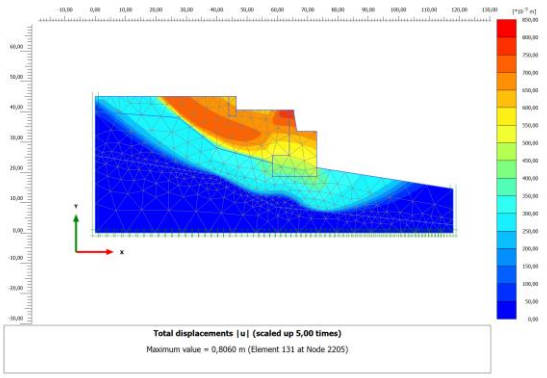

Figure 15. Total displacements of the MSPA not considering interfaces with a horizontal acceleration of 0,50g

The maximum calculated displacement is equal to ~0,81 m and in Figure 15. It can be seen that the same compound slip surface appears, and there are no major displacements detected in GZ3. In fact the larger displacements are appear in GZ1, which indicated that in case of failure, GZ1 would be the one that slides.

6. Concluding remarks

The lower retaining wall of the MSPA presents two patterns of movement were observed between 2010 and 2012. The patterns are (i) sinusoidal variations with a period of one year, and (ii) an increasing displacement in the transversal direction, accumulating ~14 mm displacement in three years. Additionally, the inclinometers identified relative motion ~24 m deep near the interface between two geotechnical zones. The increasing displacements seem to be described by a forming compound slip surface under the MSPA.

Using the Fukuzono (1985) method to predict a time of failure for the point that presented the larger displacements lead to short term failure, that it is known that did not happen.

The three possible causes for the displacements observed and its analysis are summarized in Table 4. The causes of movement presented explain part of the displacements observed in the MSPA and its trend.

Although there are various causes for the increasing displacements in the MSPA, all these hypotheses lead to a similar compound slip surface: planar bellow the MSPA and circular after the lower retaining wall with larger displacements in the lower platform and GZ1, concluding that in case of rupture this slip surface is the more likely to occur.

Table 4. Possible causes of displacement of the MSPA

Causes of movement	Comments
Precipitation	Precipitation seems to be the origin of the seasonal displacements observed. However, it does not seem to be the cause of the increasing displacements observed in the transversal direction.
Earthquakes	Based on the measured displacements, the M4,2 earthquake did not have an impact on the MSPA displacements. In the numerical model proposed, the MSPA collapses for accelerations over 0,50g that corresponds to very strong earthquake.
Forming slip surface between GZ2 and GZ3	In the displacements measured by the inclinometers a possible slip surface between GZ2 and GZ3 was identified, and its impact on the MSPA displacements was confirmed by the numerical model. Although this slip surfaces explains the trend of the displacements it does not explain their amplitude. The cause for a weaker interface is not easy to explain, because the area was built more a century ago.
Stiffness reduction in GZ2	The stiffness reduction in GZ2 generates a displacement profile similar to the one measured in the inclinometers in shape, but the amplitude of the displacements is significantly smaller.

References

Cruden, D. M. (1991). A Simple Definition of a Landslide. In *Bulletin of the International Association of Engineering Geology Nº43* (pp. 27–29).

Fukuzono, T. (1985). A method to predict the time of slope failure caused by rainfall using the inverse number of velocity of surface displacement. *Journal of Japan Landslide Society, 22*(2), 8–13.

Geoide. (2017). *Monitorização Topográfica*.

Geotest. (2011). *Miradouro de S. Pedro de Alcântara - Lisboa Estudo Geológico e Geotécnico Relatório.*

Geotest, (2016). *Relatório VIII de Leituras em Tubos Inclinométricos e Piezométricos.*

Intrieri, E., Carlà, T., & Gigli, G. (2019). Forecasting the time of failure of landslides at slope-scale: A literature review. *Earth-Science Reviews, 193,* 333–349.

Intrieri, E., & Gigli, G. (2016). Landslide forecasting and factors influencing predictability. *Natural Hazards and Earth System Sciences, 16*(12), 2501–2510.

IPMA (Instituto Portugês do Mar e da Atmosféra). (n.d.). *Portugal ShakeMap: Estimated Instrumental Intensity.* Retrieved August 9, 2020, from http://shakemap.ipma.pt/2017081706445801/intensity.html

Kulhawy, F. H., & Mayne, P. W. (1990). Manual on Estimating Soil Properties for Foundation Design. In *EPRI Report EL-6800*.

Lacasse, S., & Nadim, F. (2009). Landslide risk assessment and mitigation strategy. *Landslides - Disaster Risk Reduction*, 31–62.

Laranjo, M. (2013). *Argilas Miocénicas de Lisboa Parametrização para o Dimensionamento de Estruturas Geotécnicas*. Faculdade de Engenharia, Universidade do Porto. PhD Thesis.

Mufundirwa, A., Fujii, Y., & Kodama, J. (2010). A new practical method for prediction of geomechanical failure-time. *International Journal of Rock Mechanics and Mining Sciences, 47*(7), 1079–1090.

Oliveira, L. (n.d.). *Seismic microzonation studies for Lisbon*. Faculdade de Ciências, Universidade de Lisboa. PhD Thesis. Under preparation. PhD Thesis (expected 2022)

Saito, M. (1969). Forecasting time of slope failure by tertiary creep. *7th International Conference on Soil Mechanics and Foundation Engineering, 2*, 677–683.

Teixeira Duarte Engenharia, S. A. (2017). *Miradouro de São Pedro de Alcântara - III Séculos de História.*